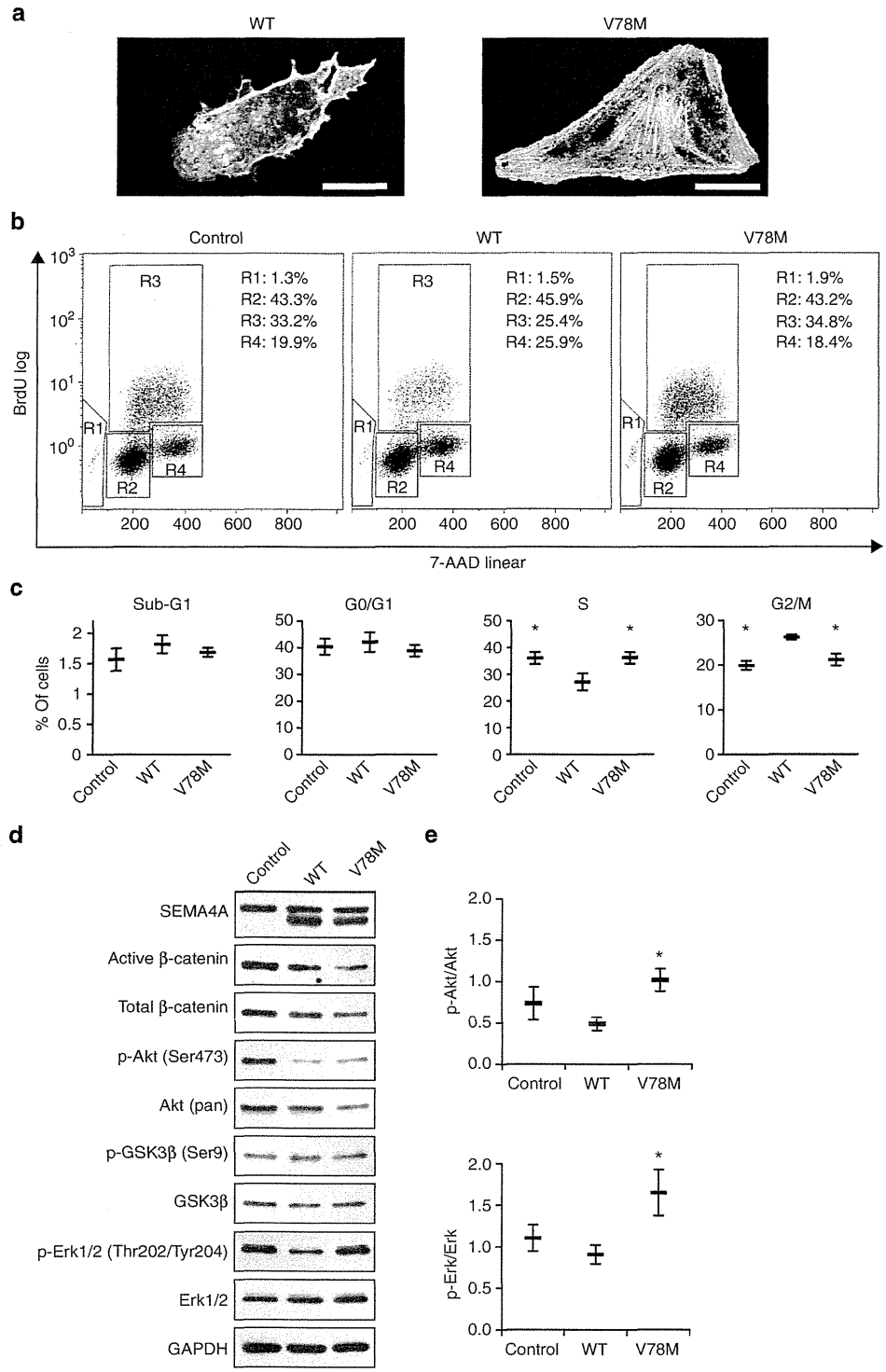

Figure 4 | SEMA4A^{V78M} shows normal surface expression and leads to cell cycle changes in HCT-116 cells. (**a**) ARPE-19 cells were transfected with the plasmid constructs expressing Sema4A^{WT}-EGFP or Sema4A^{V78M}-EGFP proteins, incubated for 48 h and stained with phalloidin. Green, Sema4A-EGFP; red, phalloidin (actin). Representative images obtained by confocal microscopy are shown. The size of the scale bar is 20 μm. (**b**,**c**) Representative density plots and statistical analysis of GFP-positive SEMA4A-transfected HCT-116 cells stained by 7-AAD and APC anti-BrdU antibodies for cell cycle analysis. Cells were analysed 48 h after transfection. Significantly, more SEMA4A^{V78M} than SEMA4A^{WT}-transfected cells are in S phase and significantly less in G2/M phase, respectively (mean ± s.e.m.; $n=3$ per group; two-tailed paired Student's *t*-test; $^*P<0.05$ compared with WT). Cell cycle phase: Sub-G1 (R1), G1/G0 (R2), S (R3), G2/M (R4). (**d**,**e**) Representative immunoblots and statistical analysis of SEMA4A-transfected HCT-116 cells (whole-cell lysates) lyzed 48 h after transfection. SEMA4A^{V78M}-transfected cells show increased phosphorylation of Akt and Erk (mean ± s.e.m.; $n=6$ per group; two-tailed paired Student's *t*-test; $^*P<0.05$ compared with WT). (p-)GSK3β and (active) β-catenin proteins were blotted on a separate membrane in this experiment. No effects on GSK3β and β-catenin phosphorylation were seen in repeated experiments.

Table 3 | Results of the *SEMA4A* Pro682Ser association study.

Cohort*	No.	Genotypes			Frequency of allele T (%)	Two-tailed *P* value†	OR (95% CI)
		CC	CT	TT			
German and Austrian FCCTX individuals	47	41	6	0	6.4	0.0008	6.793 (2.634 to 17.518)
Non-cancer controls‡	1,138	1,114	24	0	1.1	—	1

CI, confidence interval; FCCTX, familial colorectal cancer type X; OR, odds ratio.
*Genotypes of cases and controls were in Hardy-Weinberg equilibrium, with *P* values (df = 1) of 0.718 and 0.647, respectively.
†Fisher's exact test of genotype counts from cases versus controls.
‡Men, *n* = 574 (50.4%); women, *n* = 564 (49.6%); mean age: 60 years (± s.d. 18); median age: 64 years (range 15–99).

interpreted this way, should be handled with extreme caution as context specific functions have to be taken into account. Indeed, it has recently been shown that solubilized Sema4A at high levels is able to suppress cell death induced by plexin D1 in the mouse mammary tumour cell line 4T1, whereas the identical constellation inhibited proliferation in human endothelial cells[16,39].

Our *in vitro* results have shown that SEMA4A^{V78M} differentially modulates the PI3K/Akt and MAPK/Erk pathways in HCT-116 cells and that additional molecular hits are likely needed to establish the SEMA4A^{V78M} phenotype, which is in accordance with well-established concepts of predisposing germline mutations[37]. For instance, mutations in the *PIK3CA* and *KRAS* genes found in the HCT-116 cell line could represent additional oncogenic hits. Recently, two different molecular entities have been postulated among FCCTX families with respect to somatically acquired aberrations found in their CRCs. One entity exhibiting loss of tumour suppressor loci involving the *TP53*, *APC*, *SMAD4* and *DCC* genes as well as mutations in *APC* and *KRAS* and another one with stable genotypes at these loci[40–42]. Although our data demonstrating somatic mutations in the *TP53*, *APC* and *KRAS* genes in CRCs from Family K are in line with these results, the numbers of tumours studied are too small to draw a final conclusion especially with respect to cooperation with SEMA4A^{V78M}.

In summary, the data presented here broaden our understanding of the pathophysiological role of semaphorins in human carcinogenesis and will have important consequences for screening and early tumour detection strategies of patients with FCCTX and their family members.

Methods

Subjects and primary samples. The study was approved by the institutional review board of the Medical University of Graz, Graz, Austria (MUG) and conducted according to the declaration of Helsinki. Written informed consent was obtained from each study participant or, in the case of deceased patients, close relatives for providing personal and family history data as well as biological specimens. Some of them were processed and stored by the Biobank of MUG.

Family K (germline *SEMA4A* p.Val78Met) was from southern Austria and consisted of 88 members spread into two branches. Clinical data revealed that AC-I criteria compatible with HNPCC (LS) were fulfilled (Fig. 1a; Supplementary Fig. 1). However, CRCs from two patients in either branch (K13 and K26) showed normal expression of the DNA MMR genes *MLH1*, *MSH2*, *MLH6* and *PMS2* by immunohistochemistry as well as microsatellite stability. Furthermore, in individual K13, tumour tissue revealed absence of a somatically acquired *BRAF* mutation. Large germline rearrangements in the MMR genes and *EPCAM*, respectively, as a rare cause of HNPCC were also excluded by multiplex ligation-dependent probe amplification in this patient. We, therefore, made a diagnosis of FCCTX in this family.

To prove that *SEMA4A* germline mutations are also operable in other patients with FCCTX, we studied a cohort of 53 further cases with this syndrome (Supplementary Table 3). Clinical data as well as DNA extracted from PB were provided by the German HNPCC Consortium, Bonn, Germany ($n = 44$), the Division of Gastroenterology, Baylor University Medical Center, Dallas, Texas, USA ($n = 6$) and the Institute of Human Genetics, MUG ($n = 3$) in accordance with local ethical guidelines. One patient (MUG1) fulfilled the modified AC criteria[4], whereas all others, classical AC-I and/or AC-II criteria.

Index patient BN01 with germline *SEMA4A* p.Ser326Phe mutation had microsatellite stable sigmoid colon cancer. Index patient BN04 identified to carry the germline *SEMA4A* p.Gly484Ala mutation has been analysed for germline mutations in *MLH1*, *MSH2*, *MLH6* and *PMS2* by direct sequencing which revealed negative results. Her brother's CRC (III:IV) showed low microsatellite instability.

DNA and RNA isolation. DNA purification from PB mononuclear cells, cell lines and fresh frozen tissue specimens were accomplished with the QIAamp DNA Mini Kit (Qiagen) according to the manufacturer's instructions. The RNeasy Mini Kit (Qiagen) was used for RNA isolation from PB mononuclear cells and cell lines. To investigate tumour-specific aberrations, tumour-bearing tissue was manually microdissected from archival, FFPE specimens and DNA isolated using the ReliaPrep FFPE gDNA Miniprep kit (Promega).

Genotyping and LA. LA was performed in Family K afflicted with FCCTX (Fig. 1a; Supplementary Fig. 1). The GeneChip Human Mapping 250 K Nsp Array (Affymetrix) was used for genotyping of family members according to the manufacturer's protocols. A genome-wide analysis of linkage was conducted under the assumption of an autosomal dominant mode of inheritance with assignment of phenotype to persons affected by the trait (K3, K6, K10, K14, K13, K18) and with additional inclusion of one spouse of one affected person (K15) for improved haplotype reconstruction. The disease allele was assigned a frequency of 0.001 and 100% penetrance for multipoint parametric LA on this subset of family members which was performed with the MERLIN programme in the Alohomora Linkage software tool[43,44].

Whole exome sequencing and data analysis. WES and analysis were performed in four members of the family (K3, K13, K14, K18). Each patient DNA was prepared according to the Illumina protocols. Briefly, 1 µg of genomic DNA was fragmented and Illumina adaptors were ligated to the fragments. Selected DNA fragments with a size of 350 to 400 bp were then PCR amplified using the TruSeq DNA Sample Preparation kit (Illumina), and the final products were analysed for integrity by the Agilent Bioanalyzer. Multiple DNA libraries were combined with different indices into a single pool before enrichment. Hybridization with capture probes, washing and eluting were performed two times. Enriched targeted regions were amplified by PCR using the same primers from the TruSeq DNA Sample Preparation kit and then sequenced on a HiSeq 2000 Sequencer (Illumina).

Sequence data in FastQ format were aligned to the hg19 version of the human genome (GRCh37) using the Burrows-Wheeler Aligner[45] (BWA; http://bio-bwa.sourceforge.net/), transformed into SAM files and then converted into compressed BAM files by picard (http://picard.sourceforge.net/). Possible PCR duplicates were marked by picard and local realignment around indels was performed using the Genome Analysis Tool Kit[46] (GATK; http://www.broadinstitute.org/gatk/download) to prevent false positive SNPs at the end of sequence reads. GATK was also used to reevaluate base quality scores, perform the raw SNP calling of all sequences within RefSeq gene exons (http://www.ncbi.nlm.nih.gov/RefSeq/) - plus ten bp at each splice site—and to recalibrate variant quality scores.

With a read length of 101 bp, there were, on average, 88,333,643 total reads that could be mapped to the human genome in 64.5%, respectively. The mean read depth of target regions (96.4% of RefSeq (refGene) coding exons and 97.2% of CCDS coding exons, respectively) was 49.1 × . The mean coverage of target regions more than 1 × was 94.5% and the mean coverage of target regions more than 10 × was 87.3%, respectively.

Variant calls were annotated with ANNOVAR[47] (http://www.openbioinformatics.org/annovar/), which contained the data from dbSNP132 (http://www.ncbi.nlm.nih.gov/SNP/) and the allele frequencies of the 1000 Genomes Project from February 2012 (http://www.1000genomes.org/) and of the ESP5400 version of the NHLBI GO Exome Sequencing Project (https://esp.gs.washington.edu/drupal/). During progression of the study, variants were also manually checked for frequencies in updated versions of those databases. Furthermore, single variants were analysed by the following prediction programs: SIFT (http://sift.jcvi.org/), Polyphen-2 (http://genetics.bwh.harvard.edu/pph2/), MutationTaster 2.0 (http://www.mutationtaster.org/), PhyloP, phastCons and GERP (the last three were precalculated from the UCSC genome browser http://genome.ucsc.edu/cgi-bin/hgGateway). An in-house databank consisting of 18 exomes sequenced on the Illumina platform was used to exclude sequence artifacts as well as variants not covered extensively by public databases. The median age of

individuals was 23 years (range 4 to 75 years) and they all are obtained from families lacking a personal or family history of cancer. Variants were excluded if they were found in at least two individuals from the in-house databank, variants found in only one individual were further checked by functional prediction tools.

Variant resequencing and screening of SEMA4A. Confirmation of mutations detected at WES and screening of the *SEMA4A* gene in 53 further patients with FCCTX were accomplished by PCR and Sanger sequencing. Oligonucleotide primers were designed with Primer-BLAST (http://www.ncbi.nlm.nih.gov/tools/primer-blast/) or ExonPrimer (http://ihg.helmholtz-muenchen.de/ihg/ExonPrimer.html), respectively. Primers for resequencing were designed to cover the variant and have a size preferably smaller than 300 bp. All 14 coding exons as well as intron–exon boundaries of the *SEMA4A* gene were analysed. Primers used in this screening are summarized in Supplementary Table 6. They were tagged by M13 sequences to facilitate direct sequencing. PCRs were performed using the Hot-StarTaq DNA Polymerase (Qiagen) or the peqGOLD Hot Start Mix S (PEQLAB), respectively. Capillary electrophoresis was performed on ABI PRISM 3730 DNA Analyzer or ABI PRISM 310 Genetic Analyzer, respectively (both by Applied Biosystems). Chromatograms were analysed with FinchTV v.1.4.0 (Geospiza) and SeqScape software v.2.5 (Applied Biosystems).

Reverse transcription and SEMA4A cDNA amplification. RNA (1 μg) was digested with DNase I, RNase-free (Thermo Scientific) and reversely transcribed with random hexamer primers using the RevertAid H Minus First Strand cDNA Synthesis Kit (Thermo Scientific). A negative control (RT-minus) was always included. Primers for amplification of the reference gene *B2M* were as previously described[48]. Primers for *SEMA4A* transcript variants were as follows: var1-3fw, 5′-CCTGGGCCTTTTCCTCTTCC-3′; var124fw, 5′-TTTCTCCTGAATGGCAC CCC-3′; var1-4rv, 5′-TTTTTCTGTCACTGGCTGGC-3′ (the reverse primer was the same for all transcript variants). Primers var1-3fw and var1-4rv were also used for direct sequencing of amplified cDNA to assess mRNA expression of the V78M variant.

Genotyping of *SEMA4A* Pro682Ser. We determined the frequency of *SEMA4A* P682S in a normal Caucasian population and performed a genetic association analysis. Genotypes were determined by a 5′-exonuclease assay (TaqMan). Primer and probe sets were designed and manufactured using Applied Biosystems 'Assay-by-Design' custom service (Life Technologies, USA). General TaqMan reaction conditions were set according to the manufacturer's instructions. Endpoint fluorescence was measured by the POLARstar plate reader (BMG Labtech). The data were exported into an Excel format and depicted and analysed as scatter plot. In this plot, genotype groups were identified as separate and distinguishable clusters. As a control for consistency of genotyping methods, determination of genotypes was repeated in at least 10% of the samples and no discrepancies were observed. Fisher's exact test was used to test for association of genotypes from cases with genotypes from controls (GraphPad Quickcalc online; http://graphpad.com/quickcalcs/contingency1.cfm). Hardy–Weinberg equilibrium testing of cases and control was performed as previously described[49]. Odds ratios were calculated using MedCalc (http://www.medcalc.org/calc/odds_ratio.php).

Somatic cancer gene mutation screening. Selected target regions of 50 tumour-associated genes, corresponding to 2,855 COSMIC annotated hot spot mutations, were amplified by multiplexed PCR using the IonAmpliSeq Cancer Hotspot Panel v2 (Thermo Fisher Scientific). Library preparations were performed using the Ion AmpliSeq Library Kit 2.0 (Thermo Fisher Scientific). Emulsion PCR and sequencing were performed with the appropriate kits (Ion One Touch Template Kit v2 and Ion Proton 200 Sequencing Kit, (both from Thermo Fisher Scientific), respectively) on an Ion Torrent Proton sequencer using a single P1 semiconductor chip yielding reads ranging from 90 to 130 bp consistent with the expected PCR fragment size-range. On average, one million reads were obtained for each sample with more than 90% of bases above AQ20 and 87 to 93% reads on-target. Sequence information was obtained from tumour samples in duplicates and additionally from normal non-tumour material.

Initial data analysis was performed using the Ion Torrent Suite Software (Thermo Fisher Scientific, open source, GPL, https://github.com/iontorrent/). Briefly, this included base calling, alignment to the reference genome (hg19) using the TMAP mapper and variant calling with a modified diBayes approach taking into account the flow space information. All called variants were annotated using open source software[47,50] (ANNOVAR, http://www.openbioinformatics.org/annovar/; SnpEff, http://snpeff.sourceforge.net/) and custom Perl scripts. Coding, non-synonymous sequence variations that were detected and confirmed in tumours but not in the normal tissue were further evaluated and visually inspected in IGV (http://www.broadinstitute.org/igv/) to exclude erroneous variant calls resulting from PCR artifacts or sequence effects. The detection threshold was set to 10% mutated alleles in both duplicates.

Array comparative genomic hybridization. Tumour DNA samples were labelled using the BioPrime Array CGH Genomic Labeling System (Invitrogen) according to manufacturer's protocol. Briefly, 250 ng of AluI and RsaI digested tumour and reference DNA (Promega) were differentially labelled with dCTP-Cy5 and dCTP-Cy3, respectively (GE Healthcare) and purified by Amicon Ultra-0.5 30kDA filters (Millipore). Analysis of DNA copy-number changes was conducted using a SurePrint G3 60K array (Agilent) scanned on the microarray scanner G2505B (Agilent) according to the manufacturer's instructions. Feature Extraction and DNA Workbench softwares (Agilent) were used for data analysis.

Digital PCR. The *SEMA4A* V78M mutation was quantitatively analysed with digital PCR (dPCR) on the QuantStudio 3D platform (Life Technologies). A Custom TaqMan SNP Genotyping Assay specific for the analysis of the V78M mutation was used and tested on a StepOne Plus instrument (Life Technologies) using the TaqMan Genotyping Master Mix (Life Technologies) according to the manufacturer's recommendations. For dPCR, 17.4 μl of Digital PCR Master Mix (2 ×) was mixed with 1.7 μl of the TaqMan assay and 60 ng of DNA to a final volume of 36 μl and subjected to two Digital PCR 20k Chips. The chips were thermally cycled in a two-step PCR using the GeneAmp PCR System 9700 (10 min 96 °C, followed by 44 cycles of 56 °C 2 min and 94 °C 30 s, final extension of 2 min 58 °C) and imaged in the QuantStudio 3D instrument. Raw data were analysed using the Relative Quantification module of the QuantStudio 3D AnalysisSuite Software. The confidence level was set to 95% and the desired precision value was 10%.

Cell culture. Adherent cell lines HT-29, SW-480, HCT-116, HRT-18 and 293T were obtained from ATCC and cultivated for a maximum of 6 weeks in DMEM (Sigma-Aldrich) supplemented with 10% (v/v) HyClone fetal bovine serum (Thermo Scientific) and 1X Antibiotic-Antimycotic (Life Technologies) in a humidified chamber at 37 °C and 5% CO_2. The identity of all cell lines was confirmed by VNTR analysis using the AmpF/STR Profiler Plus Kit and ABI PRISM 310 Genetic Analyzer (both by Applied Biosystems, respectively) according to the manufacturer's protocols and verified at the online service of the DSMZ cell bank (http://www.dsmz.de).

Vectors and transfection. pReceiver-M46 (C-Flag + IRES-eGFP) control, *SEMA4A* wild-type and *SEMA4A* V78M mutated vectors were purchased from GeneCopoeia and propagated in One Shot TOP10 Chemically Competent *E. coli* (Life Technologies). Plasmids were purified by JETSTAR Maxi Plasmid Purification Kit (Genomed) and checked by direct sequencing. One day before transfection, 6×10^5 cells were seeded into six-well tissue culture plates to achieve 60 to 80% confluency. Plasmid and Lipofectamine LTX (Life Technologies) were diluted at a ratio of 1:10 (HCT-116) or 1:5 (293T), respectively, in 500 μl serum-free Opti-MEM medium (Life Technologies) for transfection. If not indicated otherwise, cells were usually grown for 48 h after transfection before whole-cell lysate preparation.

Whole-cell lysates and immunoblotting. Protein preparations were performed at 4 °C. After washing cells two times with PBS, whole-cell lysates were produced from culture dish attached adherent cells using RIPA Buffer (Sigma-Aldrich) supplemented with 2 × Halt Protease Inhibitor and 2 × Halt Phosphatase Inhibitor Cocktails (Thermo Scientific) which were added just before lysis. Adherent cells were scraped from the plate after incubating on a shaker for 5 to 15 min and subsequently quickfrozen in liquid nitrogen and submitted to two freeze-thaw cycles. Lysate were clarified by centrifugation at 8,000 *g* for 10 min.

Protein concentration was determined with the DC Protein Assay (Bio-Rad) using SPECTROstar Omega and MARS Data Analysis Software (both BMG LABTECH). Lysates were diluted with 4 × Laemmli sample buffer (Bio-Rad) and 710 mM final β-mercaptoethanol and incubated for 5 min at 95 °C. SDS-Polyacrylamide gel electrophoresis of equal protein amounts was performed with precast Mini-PROTEAN TGX 4-15% gels (Bio-Rad). Proteins were blotted onto low fluorescence PVDF transfer (Advansta) or Supported Nitrocellulose (Bio-Rad) membranes, respectively. Membranes were blocked with 3% (wt/v) Non-Fat Dry Milk in TBS (Bio-Rad) with 0.01% (v/v) Tween 20 (Sigma-Aldrich). Proteins were detected with specific primary antibodies directed at: SEMA4A (1:200, #sc-67073, Santa Cruz Biotechnology), Active-β-Catenin (1:1,000, #05-665, Millipore), β-Catenin (1:200, #sc-1496, Santa Cruz Biotechnology), Akt (pan) (1:1,500, #4691, Cell Signaling), Phospho-Akt (Ser473) (1:2,000, #4060, Cell Signaling), p44/42 MAPK (Erk1/2) (1:2,500, #4695, Cell Signaling), Phospho-p44/42 MAPK (Erk1/2) (Thr202/Tyr204) (1:2,000, #4370, Cell Signaling), GSK-3β (1:1,500, #9832, Cell Signaling), Phospho-GSK-3β (Ser9) (1:3,000, #5558, Cell Signaling), GAPDH (1:2,000, #sc-32233, Santa Cruz Biotechnology). Horseradish peroxidase-linked secondary antibodies were anti-rabbit IgG (#7074, Cell Signaling) and anti-mouse immunoglobulins (#P026002, Dako), both diluted 1:10,000, respectively. Membranes were incubated in Restore Plus Western Blot Stripping Buffer (Thermo Scientific) at 37 °C to strip antibodies. Imaging of blots was performed by chemiluminescence using WesternBright ECL horse radish peroxidase substrate (Advansta), CL-XPosure films (Thermo Scientific) and CURIX 60 developer (Agfa Healtcare), respectively. ImageJ 1.47v (NIH, rsbweb.nih.gov/ij) was used for analysis of band densities.

Surface expression studies. Analysis of Sema4A surface expression in ARPE-19 cells was performed as previously described[18]. The cDNA sequence encoding full-length mouse Sema4A (amino acids 1–760) was generated by PCR and then ligated into pEGFP-N3 (Clontech, Palo Alto, CA). Mutant Sema4AV78M-EGFP construct was generated from Sema4AWT-EGFP using a QuikChange II XL site-directed mutagenesis kit (Stratagene) according to the manufacturer's protocol. Cells were transfected using FuGENE HD (Roche).

Migration assay. A cell exclusion zone migration assay was performed with the Radius 24—Well Cell Migration Assay plate (Cell Biolabs) according to the manufacturer's instructions. Briefly, HCT-116 cells were seeded into 60 mm cell culture dishes and transfected with control and SEMA4A vectors. Six hours after transfection, cells from one 60-mm dish were split into four wells of one assay plate and grown overnight to allow attachment at full confluency. Time lapse microscopy was started 24 h post transfection by removing the gel spot and concurrent switching of medium to DMEM with 1% (v/v) fetal bovine serum. Cells were monitored for 48 h with a 1-h interval by the Cell Observer (Carl Zeiss). ImageJ 1.47v was used for analysis of cell migration. Closed areas were calculated for each well at different time points by subtracting the open surface area at a given time point from the open surface area at the beginning of the migration assay.

7-AAD/BrdU staining and flow cytometry. Twenty-four hours after transfection in 35 mm dishes as described, 1.5×10^6 HCT-116 cells were transferred to 100 mm cell culture dishes and grown for approximately 24 h under normal conditions. BrdU at a final concentration of 50 μM was then added and cells were incubated for 1 h protected from light to label actively proliferating cells. One million cells were washed with ice cold PBS by centrifugation at 4 °C and then fixed for 30 min at room temperature, permeabilized for 10 min on ice, refixed for 5 min at room temperature, treated with DNase and finally stained with APC anti-BrdU antibody (1:50 for 30 min at room temperature) as well as 7-AAD according to the instructions from the APC BrdU Flow Kit (BD Pharmingen). Unlabelled native cells were used as a negative control for the APC anti-BrdU antibody. Stained cells were acquired on the BD LSR II Flow Cytometer operated with FACSDiva Software (both from BD Biosciences, respectively) with a flow rate of less than 400 cells s^{-1} on the same day of staining. Kaluza Flow Cytometry Analysis Software v1.2 (Beckman Coulter) was used for analysis and illustration of flow cytometry data.

Multiple sequence alignment and 3D modelling of SEMA4A. Multiple sequence alignment was performed with Clustal Omega (http://www.clustal.org/omega/). Structural models of SEMA4A containing the SEMA and PSI domains only (amino acids 55 to 527 in NP_001180229.1 reference sequence) were generated using the intensive model algorithm of phyre2 (ref. 51) and drawn by POLYVIEW-3D (http://polyview.cchmc.org/polyview3d.html).

Statistics. Results obtained from experiments with isogenic cell lines were compared in Excel 2013 using a paired, two-tailed Student's *t*-test.

References

1. Siegel, R., Desantis, C. & Jemal, A. Colorectal cancer statistics, 2014. *CA-Cancer. J. Clin.* **64,** 104–117 (2014).
2. Jasperson, K. W., Tuohy, T. M., Neklason, D. W. & Burt, R. W. Hereditary and familial colon cancer. *Gastroenterology* **138,** 2044–2058 (2010).
3. Lynch, H. T. *et al.* Review of the Lynch syndrome: history, molecular genetics, screening, differential diagnosis, and medicolegal ramifications. *Clin. Genet.* **76,** 1–18 (2009).
4. Umar, A., Risinger, J. I., Hawk, E. T. & Barrett, J. C. Testing guidelines for hereditary non-polyposis colorectal cancer. *Nat. Rev. Cancer* **4,** 153–158 (2004).
5. Lindor, N. M. *et al.* Lower cancer incidence in Amsterdam-I criteria families without mismatch repair deficiency: familial colorectal cancer type X. *JAMA* **293,** 1979–1985 (2005).
6. Steinke, V. *et al.* Evaluating the performance of clinical criteria for predicting mismatch repair gene mutations in Lynch syndrome: a comprehensive analysis of 3671 families. *Int. J. Cancer* **135,** 69–77 (2014).
7. Lindor, N. M. Familial colorectal cancer type X: the other half of hereditary nonpolyposis colon cancer syndrome. *Surg. Oncol. Clin. N. Am.* **18,** 637–645 (2009).
8. Mueller-Koch, Y. *et al.* Hereditary non-polyposis colorectal cancer: clinical and molecular evidence for a new entity of hereditary colorectal cancer. *Gut.* **54,** 1733–1740 (2005).
9. Engel, C. *et al.* Risks of less common cancers in proven mutation carriers with lynch syndrome. *J. Clin. Oncol.* **30,** 4409–4415 (2012).
10. Schulz, E. *et al.* Germline mutations in the DNA damage response genes BRCA1, BRCA2, BARD1 and TP53 in patients with therapy related myeloid neoplasms. *J. Med. Genet.* **49,** 422–428 (2012).
11. Sill, H., Olipitz, W., Zebisch, A., Schulz, E. & Wolfler, A. Therapy-related myeloid neoplasms: pathobiology and clinical characteristics. *Br. J. Pharmacol.* **162,** 792–805 (2011).
12. Farrington, S. M. *et al.* Germline susceptibility to colorectal cancer due to base-excision repair gene defects. *Am. J. Hum. Genet.* **77,** 112–119 (2005).
13. Yurgelun, M. B. *et al.* Microsatellite instability and DNA mismatch repair protein deficiency in Lynch syndrome colorectal polyps. *Cancer Prev. Res. (Phila)* **5,** 574–582 (2012).
14. Kumanogoh, A. *et al.* Nonredundant roles of Sema4A in the immune system: defective T cell priming and Th1/Th2 regulation in Sema4A-deficient mice. *Immunity* **22,** 305–316 (2005).
15. Delgoffe, G. M. *et al.* Stability and function of regulatory T cells is maintained by a neuropilin-1-semaphorin-4a axis. *Nature* **501,** 252–256 (2013).
16. Toyofuku, T. *et al.* Semaphorin-4A, an activator for T-cell-mediated immunity, suppresses angiogenesis via Plexin-D1. *EMBO J.* **26,** 1373–1384 (2007).
17. Abid, A., Ismail, M., Mehdi, S. Q. & Khaliq, S. Identification of novel mutations in the SEMA4A gene associated with retinal degenerative diseases. *J. Med. Genet.* **43,** 378–381 (2006).
18. Nojima, S. *et al.* A point mutation in Semaphorin 4A associates with defective endosomal sorting and causes retinal degeneration. *Nat. Commun.* **4,** 1406 (2013).
19. Cancer Genome Atlas Network. Comprehensive molecular characterization of human colon and rectal cancer. *Nature* **487,** 330–337 (2012).
20. Mendoza, M. C., Er, E. E. & Blenis, J. The Ras-ERK and PI3K-mTOR pathways: cross-talk and compensation. *Trends Biochem. Sci.* **36,** 320–328 (2011).
21. Shtivelman, E., Sussman, J. & Stokoe, D. A role for PI 3-kinase and PKB activity in the G2/M phase of the cell cycle. *Curr. Biol.* **12,** 919–924 (2002).
22. Shinohara, M., Mikhailov, A. V., Aguirre-Ghiso, J. A. & Rieder, C. L. Extracellular signal-regulated kinase 1/2 activity is not required in mammalian cells during late G2 for timely entry into or exit from mitosis. *Mol. Biol. Cell* **17,** 5227–5240 (2006).
23. Bahadori, B. *et al.* Polymorphisms of the hypoxia-inducible factor 1 gene and peripheral artery disease. *Vasc. Med.* **15,** 371–374 (2010).
24. Rehman, M. & Tamagnone, L. Semaphorins in cancer: biological mechanisms and therapeutic approaches. *Semin. Cell Dev. Biol.* **24,** 179–189 (2013).
25. Alexandrov, L. B. *et al.* Signatures of mutational processes in human cancer. *Nature* **500,** 415–421 (2013).
26. Neufeld, G., Sabag, A. D., Rabinovicz, N. & Kessler, O. Semaphorins in angiogenesis and tumor progression. *Cold Spring Harb. Perspect. Med.* **2,** a006718 (2012).
27. Janssen, B. J. *et al.* Structural basis of semaphorin-plexin signalling. *Nature* **467,** 1118–1122 (2010).
28. Nogi, T. *et al.* Structural basis for semaphorin signalling through the plexin receptor. *Nature* **467,** 1123–1127 (2010).
29. Croitoru, M. E. *et al.* Association between biallelic and monoallelic germline MYH gene mutations and colorectal cancer risk. *J. Natl Cancer Inst.* **96,** 1631–1634 (2004).
30. Win, A. K. *et al.* Risk of colorectal cancer for carriers of mutations in MUTYH, with and without a family history of cancer. *Gastroenterology* **146,** 1208–11.e1-5 (2014).
31. Webb, E. L., Rudd, M. F. & Houlston, R. S. Colorectal cancer risk in monoallelic carriers of MYH variants. *Am. J. Hum. Genet.* **79,** 768–771 author reply 771-2 (2006).
32. Olschwang, S., Blanche, H., de Moncuit, C. & Thomas, G. Similar colorectal cancer risk in patients with monoallelic and biallelic mutations in the MYH gene identified in a population with adenomatous polyposis. *Genet. Test.* **11,** 315–320 (2007).
33. Ismail, M., Abid, A., Anwar, K., Mehdi, S. Q. & Khaliq, S. Refinement of the locus for autosomal recessive cone-rod dystrophy (CORD8) linked to chromosome 1q23-q24 in a Pakistani family and exclusion of candidate genes. *J. Hum. Genet.* **51,** 827–831 (2006).
34. Rice, D. S. *et al.* Severe retinal degeneration associated with disruption of semaphorin 4A. *Invest. Ophthalmol. Vis. Sci.* **45,** 2767–2777 (2004).
35. Baker, S. M. *et al.* Enhanced intestinal adenomatous polyp formation in Pms2 − / − ;Min mice. *Cancer Res.* **58,** 1087–1089 (1998).
36. Takaku, K. *et al.* Intestinal tumorigenesis in compound mutant mice of both Dpc4 (Smad4) and Apc genes. *Cell* **92,** 645–656 (1998).
37. Vogelstein, B. *et al.* Cancer genome landscapes. *Science* **339,** 1546–1558 (2013).
38. Middeldorp, A. *et al.* Increased frequency of 20q gain and copy-neutral loss of heterozygosity in mismatch repair proficient familial colorectal carcinomas. *Int. J. Cancer* **130,** 837–846 (2012).
39. Luchino, J. *et al.* Semaphorin 3E suppresses tumor cell death triggered by the plexin D1 dependence receptor in metastatic breast cancers. *Cancer Cell* **24,** 673–685 (2013).
40. Sanchez-de-Abajo, A. *et al.* Molecular analysis of colorectal cancer tumors from patients with mismatch repair proficient hereditary nonpolyposis colorectal cancer suggests novel carcinogenic pathways. *Clin. Cancer Res.* **13,** 5729–5735 (2007).
41. Francisco, I. *et al.* Familial colorectal cancer type X syndrome: two distinct molecular entities? *Fam. Cancer* **10,** 623–631 (2011).

42. Dominguez-Valentin, M., Therkildsen, C., Da Silva, S. & Nilbert, M. Familial colorectal cancer type X: genetic profiles and phenotypic features. *Mod. Pathol.* doi:10.1038/modpathol.2014.49 (2014).
43. Abecasis, G. R., Cherny, S. S., Cookson, W. O. & Cardon, L. R. Merlin—rapid analysis of dense genetic maps using sparse gene flow trees. *Nat. Genet.* **30,** 97–101 (2002).
44. Ruschendorf, F. & Nurnberg, P. ALOHOMORA: a tool for linkage analysis using 10K SNP array data. *Bioinformatics* **21,** 2123–2125 (2005).
45. Li, H. & Durbin, R. Fast and accurate long-read alignment with Burrows-Wheeler transform. *Bioinformatics* **26,** 589–595 (2010).
46. DePristo, M. A. *et al.* A framework for variation discovery and genotyping using next-generation DNA sequencing data. *Nat. Genet.* **43,** 491–498 (2011).
47. Wang, K., Li, M. & Hakonarson, H. ANNOVAR: functional annotation of genetic variants from high-throughput sequencing data. *Nucleic Acids Res.* **38,** e164 (2010).
48. Beillard, E. *et al.* Evaluation of candidate control genes for diagnosis and residual disease detection in leukemic patients using 'real-time' quantitative reverse-transcriptase polymerase chain reaction (RQ-PCR) - a Europe against cancer program. *Leukemia* **17,** 2474–2486 (2003).
49. Rodriguez, S., Gaunt, T. R. & Day, I. N. Hardy-Weinberg equilibrium testing of biological ascertainment for Mendelian randomization studies. *Am. J. Epidemiol.* **169,** 505–514 (2009).
50. Cingolani, P. *et al.* A program for annotating and predicting the effects of single nucleotide polymorphisms, SnpEff: SNPs in the genome of *Drosophila melanogaster* strain w1118; iso-2; iso-3. *Fly (Austin)* **6,** 80–92 (2012).
51. Kelley, L. A. & Sternberg, M. J. Protein structure prediction on the Web: a case study using the Phyre server. *Nat. Protoc.* **4,** 363–371 (2009).

Acknowledgements

This work is dedicated to Günther J. Krejs, Professor Emeritus of Gastroenterology, Medical University of Graz, Austria. We would like to thank all patients and their family members for participating in this study. We are also grateful to Michaela Auer-Grumbach and Ian Tomlinson for critical comments, Silvia Schauer for excellent technical assistance, Wolfram Jochum for providing tumour specimens and Heinz Stammberger for supporting this project. The work was funded in part by the Austrian National Bank, Anniversary Fund (grant no. 13918), Land Steiermark, Leukämiehilfe Steiermark and 'Vereinigung Forschungsförderung' at Medical University of Graz, Austria (MUG). E.S. is supported by a dissertational grant from the Austrian Society of Hematology and Oncology and the PhD programme 'Molecular Medicine' at MUG.

Author contributions

E.S. and H.S. designed the study. E.S., P.K., A.W. and H.S. collected family data. P.K., S.Holzapfel, S.L., C.B.-S., V.S., J.B.G., C.R.B. and H.S. obtained patient samples and clinical data. A.R.J. performed the linkage analysis. P.U. analysed the whole-exome sequencing raw data. E.S., A.L. and S. Hofer performed direct sequencing. E.H. performed and analysed dPCR. K.K. performed targeted deep sequencing and analysis. C.W. provided in-house exome data. W.R. and A.G. performed and supervised genetic association analysis. E.S. and S.N. performed *in vitro* experiments. E.S., W.R., A.Z., A.W., G.H., M.R.S., A.K. and H.S. interpreted results. H.S. oversaw the study. E.S. and H.S. wrote the manuscript which was reviewed and approved by all co-authors.

Additional information

Accession codes: Raw sequencing data have been deposited in the European Genome-Phenome Archive (EGA, http://www.ebi.ac.uk/ega/) under the accession code EGAS00001000957.

Supplementary Information accompanies this paper at http://www.nature.com/naturecommunications

Competing financial interests: The authors declare no competing financial interests.

Reprints and permission information is available online at http://npg.nature.com/reprintsandpermissions/

How to cite this article: Schulz, E. *et al.* Germline variants in the *SEMA4A* gene predispose to familial colorectal cancer type X. *Nat. Commun.* 5:5191 doi: 10.1038/ncomms6191 (2014).

Efficacy of the anti–IL-6 receptor antibody tocilizumab in neuromyelitis optica

A pilot study

OPEN

Manabu Araki, MD, PhD
Takako Matsuoka, MD
Katsuichi Miyamoto, MD, PhD
Susumu Kusunoki, MD, PhD
Tomoko Okamoto, MD, PhD
Miho Murata, MD, PhD
Sachiko Miyake, MD, PhD
Toshimasa Aranami, MD, PhD
Takashi Yamamura, MD, PhD

Correspondence to Dr. Yamamura: yamamura@ncnp.go.jp

ABSTRACT

Objective: To evaluate the safety and efficacy of a humanized anti-interleukin-6 receptor antibody, tocilizumab (TCZ), in patients with neuromyelitis optica (NMO).

Methods: Seven patients with anti-aquaporin-4 antibody (AQP4-Ab)-positive NMO or NMO spectrum disorders were recruited on the basis of their limited responsiveness to their current treatment. They were given a monthly injection of TCZ (8 mg/kg) with their current therapy for a year. We evaluated the annualized relapse rate, the Expanded Disability Status Scale score, and numerical rating scales for neurogenic pain and fatigue. Serum levels of anti-AQP4-Ab were measured with AQP4-transfected cells.

Results: Six females and one male with NMO were enrolled. After a year of TCZ treatment, the annualized relapse rate decreased from 2.9 ± 1.1 to 0.4 ± 0.8 ($p < 0.005$). The Expanded Disability Status Scale score, neuropathic pain, and general fatigue also declined significantly. The ameliorating effects on intractable pain exceeded expectations.

Conclusion: Interleukin-6 receptor blockade is a promising therapeutic option for NMO.

Classification of evidence: This study provides Class IV evidence that in patients with NMO, TCZ reduces relapse rate, neuropathic pain, and fatigue. *Neurology*® 2014;82:1302-1306

GLOSSARY

Ab = antibody; **AQP4** = aquaporin-4; **AZA** = azathioprine; **EDSS** = Expanded Disability Status Scale; **IL** = interleukin; **IL-6R** = interleukin-6 receptor; **NMO** = neuromyelitis optica; **PB** = plasmablasts; **PSL** = prednisolone; **TCZ** = tocilizumab.

Neuromyelitis optica (NMO) is a relatively rare autoimmune disease that predominantly affects the spinal cord and optic nerve. Anti–aquaporin-4 antibody (AQP4-Ab), which is a disease marker of NMO, has an important role in causing the destruction of astrocytes that express AQP4.[1] Empirically, the use of disease-modifying drugs for multiple sclerosis, including interferon β, is not recommended for NMO,[2] which is consistent with the distinct pathogenesis of NMO and multiple sclerosis. We have recently described that plasmablasts (PB), which are a subpopulation of B cells, increased in the peripheral blood of patients with NMO and that PB are a major source of anti-AQP4-Ab among peripheral blood B cells.[3] In addition, we observed that exogenous interleukin (IL)-6 promotes the survival of PB and their production of anti-AQP4-Ab in vitro. Given the increased levels of IL-6 in the serum and CSF during relapses of NMO,[1,3] we postulated that blocking IL-6 receptor (IL-6R) pathways might reduce the disease activity of NMO by inactivating the effector functions of PB. A humanized anti–IL-6R monoclonal antibody, tocilizumab (TCZ) (Actemra/RoActemra), has been approved in more than 100 countries for use in the treatment of rheumatoid arthritis.[4] Herein, we describe our clinical study that aimed to explore the efficacy of TCZ in NMO.

Editorial, page 1294

From the Multiple Sclerosis Center (M.A., T.O., S.M., T.A., T.Y.) and Department of Neurology (T.O., M.M.), National Center Hospital, and Department of Immunology, National Institute of Neuroscience (T.M., S.M., T.A., T.Y.), National Center of Neurology and Psychiatry, Tokyo; Department of Neurology (K.M., S.K.), Kinki University School of Medicine, Osaka; and Department of Pediatrics (T.M.), Graduate School of Medicine, University of Tokyo, Japan.

Go to Neurology.org for full disclosures. Funding information and disclosures deemed relevant by the authors, if any, are provided at the end of the article.

Table Demographics of the patients

	Patient						
	1	2	3	4	5	6	7
Age, y/sex	37/F	38/F	26/F	31/M	55/F	62/F	23/F
Age at onset, y	23	27	21	12	38	60	21
Anti-AQP4-Ab	+	+	+	+	+	+	+
Myelitis	+	+	+	+	+	+	−
Optic neuritis	+	+	+	+	+	+	+
EDSS score	3.5	6.5	3.5	6.0	6.5	6.5	3.0
Total no. of relapses	20	9	6	16	20	3	7
ARR before TCZ	3	2	2	2	3	3	5
Immunotherapies for exacerbations	IVMP, PLEX	IVMP, PLEX	IVMP, PLEX	IVMP, OBP, PLEX	IVMP, PLEX	IVMP, PLEX	IVMP, PLEX
Past immunotherapies	IFNβ, IVIg	IFNβ	—	IFNβ, MITX	IFNβ, AZA	—	AZA
Present immunotherapies	PSL, AZA	AZA	PSL	PSL, AZA	PSL, CyA	PSL, CyA	PSL, tacrolimus
Neuropathic pain (e.g., girdle pain), NRS	4	4	2	4	4	3	0
General fatigue, NRS	5	8	6	7	5	3	9
Pain and antispasticity medication	GBP, CZP, NTP, NSAID	CZP, mexiletine, NTP, tizanidine, NSAID	—	CBZ, baclofen, NSAID	CBZ	PGB	—

Abbreviations: AQP4-Ab = aquaporin-4 antibody; ARR = annualized relapse rate; AZA = azathioprine; CBZ = carbamazepine; CZP = clonazepam; CyA = cyclosporine; EDSS = Expanded Disability Status Scale; GBP = gabapentin; IFNβ = interferon β; IVIg = IV immunoglobulin; IVMP = IV methylprednisolone; MITX = mitoxantrone; NRS = numerical rating scale; NSAID = nonsteroidal anti-inflammatory drug; NTP = Neurotropin (an extract from the inflamed skin of vaccinia virus-inoculated rabbits); OBP = oral betamethasone pulse therapy; PGB = pregabalin; PLEX = plasma exchange; PSL = prednisolone; TCZ = tocilizumab.

METHODS Level of evidence. The aim of this Class IV evidence study was to evaluate the effect and safety of a monthly injection of TCZ (8 mg/kg) with their current therapy in patients with NMO. We evaluated the adverse events based on Common Terminology Criteria for Adverse Events, version 4.0.

Standard protocol approvals, registrations, and patient consents. All patients gave written informed consent before the first treatment with TCZ. The institutional ethical standards committee on human experimentation approved this clinical study. The study is registered with University Hospital Medical Information Network Clinical Trials Registry, numbers UMIN000005889 and UMIN000007866.

Patients and treatment. Seven patients who met the diagnostic criteria of NMO in 2006 were enrolled after providing informed consent (table). Results of chest x-rays, interferon γ release assays, and plasma 1,3-β-D-glucan measurement excluded latent tuberculosis and fungal infection. All of the patients had been treated with combinations of oral prednisolone (PSL) and immunosuppressants, including azathioprine (AZA). Nevertheless, they had at least 2 relapses during the year before enrollment (figure 1). Among their past immunomodulatory medications, interferon β had been prescribed in 4 patients before the anti-AQP4-Ab assay became available. Although symptomatic treatments had been provided, the patients experienced general fatigue and intractable pain in their trunk and limbs. There were no abnormalities in their routine laboratory blood tests. Neither pleocytosis nor increased levels of IL-6 were observed in the CSF. MRI revealed high-intensity signals in the optic nerves and longitudinally extensive lesions in the spinal cord. All patients except one had scattered brain lesions. A monthly dose (8 mg/kg) of TCZ was added to the patients' oral corticosteroid and immunosuppressive drug regimen.

Clinical and laboratory assessment. As clinical outcome measures, we evaluated alterations in the number of relapses, Expanded Disability Status Scale (EDSS) scores, and pain and fatigue severity scores (numerical rating scales). A relapse was defined as an objective exacerbation in neurologic findings that lasted for longer than 24 hours with an increase in the EDSS score of more than 0.5. Brain and spinal cord MRI scans were examined every 4 or 6 months. CSF examinations, sensory-evoked potentials, and visual-evoked potentials were also evaluated at the time of entry into the study and 12 months later. We measured serum anti-AQP4-Ab levels by evaluating the binding of serum immunoglobulin G to AQP4 transfectants, as previously described.[5] All outcome measures were analyzed with nonparametric Wilcoxon rank-sum tests, with the use of 2-tailed statistical tests at a significance level of 0.05.

RESULTS After starting TCZ treatment, the total number of annual relapses in the patients significantly reduced (figures 1 and 2). Notably, 5 of the 7 patients were relapse-free after starting TCZ. The relapses observed in patients 1 and 5 were mild and their symptoms recovered after IV methylprednisolone. On average, the annualized relapse rate reduced from 2.9 ± 1.1 (range, 2–5) during the year before study to 0.4 ± 0.8 (range, 0–2) during the year after

Figure 1 Clinical course of the patients before and after tocilizumab treatment

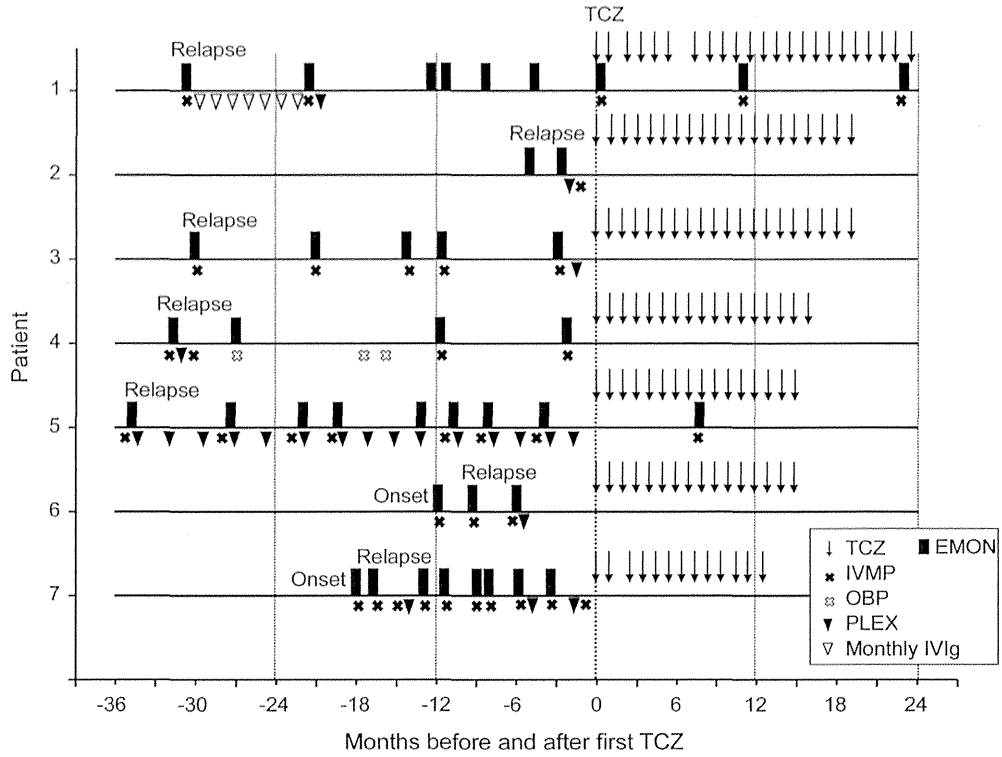

The zero on the x-axis represents the first administration of tocilizumab (TCZ). Dark gray bars: exacerbations of myelitis or optic neuritis (EMON); downward arrow: TCZ treatment; black X: IV methylprednisolone (IVMP); white X: oral betamethasone pulse (OBP) therapy; black triangle: plasma exchange (PLEX); white triangle: IV immunoglobulin (IVIg). After receiving 12 injections, all patients continued treatment with TCZ by entering an extension study that evaluates the long-term safety and efficacy of TCZ. We showed the clinical status after completion of the 1-year study to indicate the continuation of remission.

starting TCZ (figure 2). The EDSS score decreased modestly but significantly from 5.1 ± 1.7 (range, 3.0–6.5) to 4.1 ± 1.6 (range, 2.0–6.0) at 12 months. The chronic neurogenic pain in their trunk and extremities, which is characteristic of NMO[6,7] (table), gradually lessened after the patients started TCZ. Consequently, the numerical rating scale for pain reduced from 3.0 ± 1.5 upon study entry to 1.3 ± 1.3 after 6 months and 0.9 ± 1.2 after 12 months. General fatigue also improved from 6.1 ± 2.0 to 3.9 ± 2.1 at 6 months and 3.0 ± 1.4 at 12 months. The MRI scans, sensory- and visual-evoked potentials, and CSF observations did not show any interval changes. Serum anti-AQP4-Ab levels represented by the relative mean fluorescence intensity were significantly reduced (figure 2E).

Adverse events included upper respiratory infections (patients 1 and 7), acute enterocolitis (patients 1 and 4), acute pyelonephritis (patient 1), leukocytopenia and/or lymphocytopenia (patients 1, 4, and 7), anemia (patients 3 and 7), and a slight decline in systolic blood pressure (patient 1). However, none of the events was severe. Oral PSL and AZA were tapered in patients 1, 3, 4, and 7, resulting in a reduction of the mean doses (PSL from 19.5 ± 7.6 to 8.8 ± 5.6 mg/d [average of patients 1, 3, 4, and 7], AZA from 37.5 to 5.4 mg/d [average of patients 1 and 4]).

DISCUSSION Pain management is a difficult problem in patients with NMO. In fact, a retrospective study of 29 patients with NMO who experienced pain has documented that 22 of the 29 patients were taking pain medications, but none of them rated their current pain as 0 out of 10 on a 10-point scale.[6] In the present study, the intractable pain reduced gradually after the patients started TCZ treatment. After 6 or 12 months of therapy, 3 of the 6 patients with pain were completely free of pain. These results suggested a role of IL-6 in NMO pain and the possible merits of the use of TCZ in clinical practice as a pain reliever.

The pathophysiology of neurogenic pain is now understood in the context of interactions between the immune and nervous systems,[8] which involve proinflammatory cytokines such as IL-6 as well as immune cells, activated glia cells, and neurons. Supportive for the role of IL-6 in pain, recent work in

Figure 2 **Effects of tocilizumab on clinical and immunologic parameters**

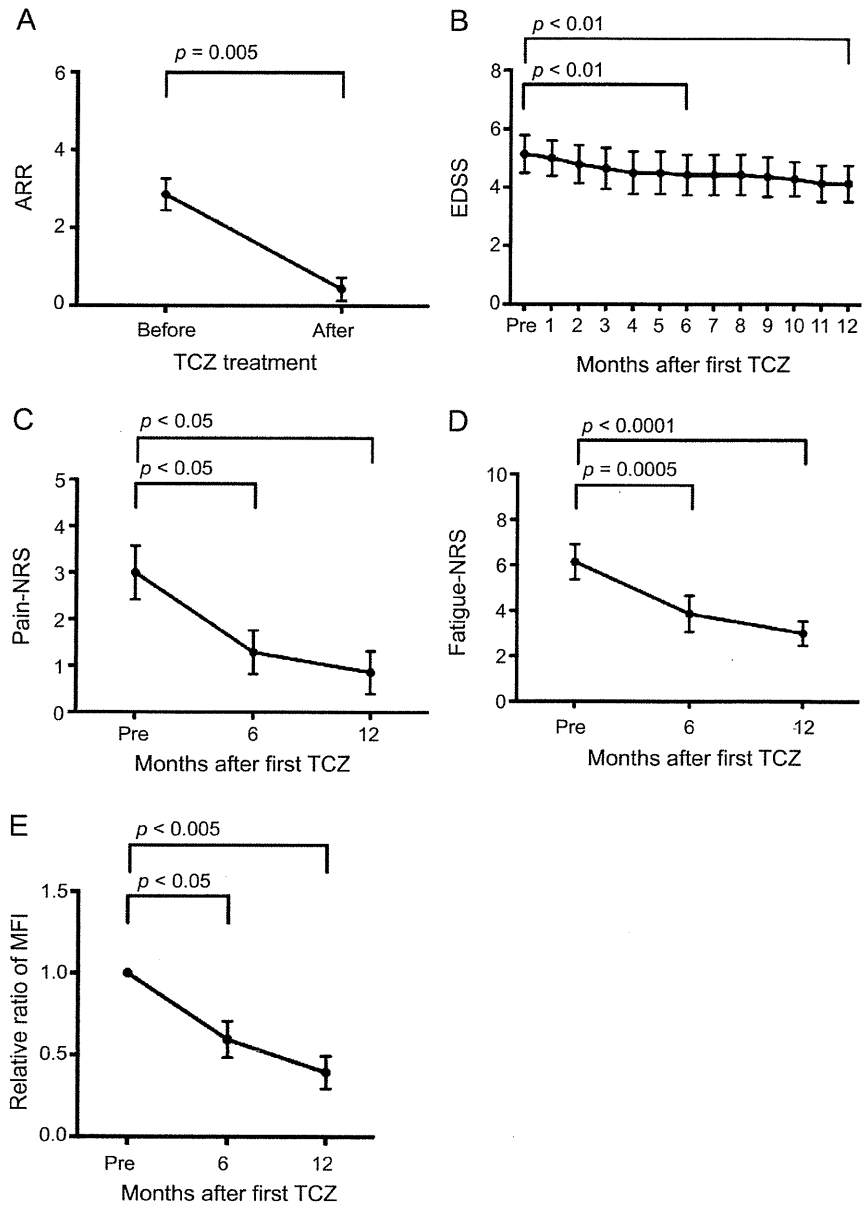

(A) Annualized relapse rate (ARR) before and after tocilizumab (TCZ) treatment. (B) Expanded Disability Status Scale (EDSS) score during the 1-year study period. Pain severity (numerical rating scale [NRS]) (C) and fatigue severity (D) scores before, 6 months after, and 12 months after the start of TCZ treatment. The dots and I bars indicate means ± SEM. We analyzed only data obtained during the first year of TCZ treatment. (E) The alterations in the serum anti-aquaporin-4 antibody (AQP4-Ab) were evaluated by the relative ratio of the mean fluorescence intensity (MFI), which was based on the MFI before TCZ treatment. Serum anti-AQP4-Ab detection assay was performed as described previously[3,5] with minor modifications. In brief, optimally diluted serum was added to human AQP4-expressing Chinese hamster ovary (CHO) cells. CHO cell-bound anti-AQP4-Ab was detected using fluorescein isothiocyanate-anti-human immunoglobulin G antibody by flow cytometry. For comparison, the MFI of each sample was divided by the MFI of the sample before the start of TCZ treatment.

rodents showed that gp130 expressed by nociceptive neurons might have a key role in pathologic pain.[9] Although expression of membrane-bound IL-6R is restricted to hepatocytes, neutrophils, and subsets of T cells, the gp130, ubiquitously expressed in cellular membranes, can transduce IL-6R signaling via binding to the IL-6/soluble IL-6R complex.[4] This indicates that IL-6 trans-signaling via the soluble IL-6R could be pivotal in causing pain in NMO, although alternative possibilities cannot be excluded.

TCZ treatment recently showed efficacy for patients with aggressive NMO who were refractory to the anti-CD20 antibody rituximab.[10] The efficacy of TCZ could result from its effect on IL-6–dependent inflammatory

processes, involving CD20-negative PB, pathogenic T cells, and regulatory T cells. This work, however, does not restrict the use of TCZ in serious NMO. Although the need for monitoring latent infection and adverse events is obvious, we propose that the use of TCZ may be considered at an early stage of NMO before disability or a lower quality of life becomes evident.

AUTHOR CONTRIBUTIONS

T.Y., S.M., S.K., M.M., and M.A.: design and conceptualization of the study. M.A., K.M., T.O., and T.Y.: analysis and internalization of the data. T.M. and T.A.: flow cytometry analysis and anti-AQP4-Ab assay. M.A. and T.Y.: drafting and revising of the manuscript. T.Y.: supervising the entire project.

STUDY FUNDING

Supported by the Health and Labour Sciences Research Grants on Intractable Diseases (Neuroimmunological Diseases) and on Promotion of Drug Development from the Ministry of Health, Labour and Welfare of Japan.

DISCLOSURE

M. Araki has received honoraria from Novartis. T. Matsuoka reports no disclosures relevant to the manuscript. K. Miyamoto has received honoraria from Novartis, Bayer, and Biogen Idec. S. Kusunoki serves as an editorial board member of *Experimental Neurology*, *Journal of Neuroimmunology*, and *Neurology & Clinical Neuroscience* (associate editor). He received honoraria from Teijin Pharma, Nihon Pharmaceuticals, Japan Blood Products Organization, Novartis Pharma, Dainippon Sumitomo Pharma, Kyowa Kirin, Asahi Kasei, Bayer, Sanofi, and GlaxoSmithKline. He is funded by research grants from the Ministry of Health, Labour and Welfare, Japan, and grants from the Japan Science and Technology Agency and the Ministry of Education, Culture, Sports, Science and Technology, Japan. He received research support from Novartis, GlaxoSmithKline, Dainippon Sumitomo Pharma, Teijin Pharma, Astellas, Sanofi, Japan Blood Products Organization, and Nihon Pharmaceuticals. T. Okamoto reports no disclosures relevant to the manuscript. M. Murata received honoraria for consulting and/or lecturing from GlaxoSmithKline Co., Ltd., Boehringer Ingelheim Co., Ltd., Dainippon Sumitomo Pharma Co., Ltd., Novartis Pharma, and Hisamitsu Pharma. S. Miyake has received speaker honoraria from Biogen Idec, Pfizer Inc., and Novartis Pharma. T. Aranami reports no disclosures relevant to the manuscript. T. Yamamura has served on scientific advisory boards for Biogen Idec and Chugai Pharmaceutical Co., Ltd.; has received research support from Ono Pharmaceutical Co., Ltd., Chugai Pharmaceutical Co., Ltd., Teva Pharmaceutical K.K., Mitsubishi Tanabe Pharma Corporation, and Asahi Kasei Kuraray Medical Co., Ltd.; has received speaker honoraria from Novartis Pharma, Nihon Pharmaceutical Co., Ltd., Santen Pharmaceutical Co., Ltd., Abbott Japan Co., Ltd./Eisai Co., Ltd., Biogen Idec, Dainippon Sumitomo Pharma Co., Ltd., Mitsubishi Tanabe Pharma Corporation, Bayer Holding Ltd., and Astellas Pharma Inc. Go to Neurology.org for full disclosures.

Received September 4, 2013. Accepted in final form December 2, 2013.

REFERENCES

1. Jarius S, Wildemann B. AQP4 antibodies in neuromyelitis optica: diagnostic and pathogenetic relevance. Nat Rev Neurol 2010;6:383–392.
2. Okamoto T, Ogawa M, Lin Y, et al. Treatment of neuromyelitis optica: current debate. Ther Adv Neurol Disord 2008;1:5–12.
3. Chihara N, Aranami T, Sato W, et al. Interleukin 6 signaling promotes anti-aquaporin 4 autoantibody production from plasmablasts in neuromyelitis optica. Proc Natl Acad Sci U S A 2011;108:3701–3706.
4. Tanaka T, Narazaki M, Kishimoto T. Therapeutic targeting of the interleukin-6 receptor. Annu Rev Pharmacol Toxicol 2012;52:199–219.
5. Araki M, Aranami T, Matsuoka T, et al. Clinical improvement in a patient with neuromyelitis optica following therapy with the anti-IL-6 receptor monoclonal antibody tocilizumab. Mod Rheumatol 2013;23:827–831.
6. Qian P, Lancia S, Alvarez E, et al. Association of neuromyelitis optica with severe and intractable pain. Arch Neurol 2012;69:1482–1487.
7. Kanamori Y, Nakashima I, Takai Y, et al. Pain in neuromyelitis optica and its effect on quality of life: a cross-sectional study. Neurology 2011;77:652–658.
8. Vallejo R, Tilley DM, Vogel L, et al. The role of glia and immune system in the development and maintenance of neuropathic pain. Pain Pract 2010;10:167–184.
9. Andratsch M, Mair N, Constantin CE, et al. A key role for gp130 expressed on peripheral sensory nerves in pathological pain. J Neurosci 2009;29:13473–13483.
10. Ayzenberg I, Kleiter I, Schröder A, et al. Interleukin 6 receptor blockade in patients with neuromyelitis optica nonresponsive to anti-CD20 therapy. JAMA Neurol 2013;70:394–397.

Arthritis & Rheumatology
DOI 10.1002/art.39086

Semaphorin 4D contributes to rheumatoid arthritis by inducing inflammatory cytokine production: pathogenic and therapeutic implications

Yuji Yoshida[1, 2], Atsushi Ogata[1, 2], Sujin Kang[2, 6], Kousuke Ebina[3], Kenrin Shi[3, 7], Satoshi Nojima[2, 4], Tetsuya Kimura[1, 2], Daisuke Ito[1, 2], Keiko Morimoto[1, 2], Masayuki Nishide[1, 2], Takashi Hosokawa[1, 2], Toru Hirano[1], Yoshihito Shima[1], Masashi Narazaki[1],Hideki Tsuboi[9], Yukihiko Saeki[10], Tetsuya Tomita[5, 8], Toshio Tanaka[1, 6] and Atsushi Kumanogoh[1, 2, 11].

[1]Department of Respiratory Medicine, Allergy and Rheumatic Diseases, Osaka University Graduate School of Medicine, Japan

[2]Department of Immunopathology, WPI Immunology Frontier Research Center, Osaka University, Japan

[3]Department of Orthopaedic Surgery, Osaka University Graduate School of Medicine, Japan

[4]Department of Pathology, Osaka University Graduate School of Medicine, Japan

[5]Department of Orthopaedic Biomaterial Science, Osaka University Graduate School of Medicine, Japan

[6]Department of Clinical Application of Biologics, Osaka University Graduate School of Medicine Japan

[7]Medical Center for Translational and Clinical Research, Osaka University Hospital, Japan

[8]Division of Orthopaedic Biomaterial Science, Osaka University Graduate School of Medicine

[9]Department of Rheumatology, National Hospital Organization Osaka Minami Medical

Received: Sep 22, 2014; Revised: Feb 05, 2015; Accepted: Feb 19, 2015

Sema4D in rheumatoid arthritis.

Center

[10]Department of Clinical Research, National Hospital Organization Osaka Minami Medical Center

[11]Core Research for Evolutionary Science and Technology (CREST), Osaka University

Corresponding to; Atsushi Ogata

Department of Respiratory Medicine, Allergy and Rheumatic Diseases, Osaka University Graduate School of Medicine, 2-2 Yamada-Oka, Suita, Osaka 565-0871, Japan

Tel: +81-6-6879-3833, fax +81-6-6879-3839

e-mail: ogata@imed3.med.osaka-u.ac.jp

Running title: Sema4D in rheumatoid arthritis.

Financial support: This study was supported by research grants and COI stream grants from the Ministry of Education, Culture, Sports, Science and Technology of Japan; grants-in-aid from the Ministry of Health, Labour and Welfare and CREST (A.K.); and JSPS KAKENHI Grant Number 25460495 (A.O.).

Conflict of interest: None

Sema4D in rheumatoid arthritis.

Abstract

Objective. Semaphorin 4D (Sema4D) /CD100 plays pleiotropic roles in immune activation, angiogenesis, bone metabolism, and neural development. This study investigated the role of Sema4D in rheumatoid arthritis (RA).

Methods. Soluble Sema4D (sSema4D) levels in the sera and synovial fluid were analyzed by ELISA. Cell-surface expression and transcripts of Sema4D were analyzed in peripheral blood cells of RA patients, and immunohistochemical staining of Sema4D was performed in RA synovium. Generation of sSema4D was evaluated in the ADAMTS4-treated monocytic cell line THP-1. The efficacy of anti-Sema4D antibody was evaluated in mouse collagen-induced arthritis (CIA).

Results. Levels of sSema4D were elevated in both sera and synovial fluid of RA patients, and disease activities were correlated with serum levels of sSema4D. Sema4D-expressing cells also accumulated in RA synovium. The cell-surface levels of Sema4D on $CD3^+$ and $CD14^+$ cells from RA patients were reduced, although the levels of *Sema4D*-transcripts were unchanged. In addition, ADAMTS4 cleaved cell-surface Sema4D to generate sSema4D in THP-1 cells. sSema4D induced tumor necrosis factor α (TNF-α) and interleukin-6 (IL-6) production from $CD14^+$ monocytes. IL-6 and TNF-α induced ADAMTS4 expression in synovial cells. Treatment with an anti-Sema4D antibody suppressed arthritis and reduced proinflammatory cytokine production in CIA.

Conclusions. A positive-feedback loop involving sSema4D/IL-6 and TNF-α/ADAMTS4 may contribute to the pathogenesis of RA. The inhibition of arthritis by anti-Sema4D antibody suggests that Sema4D represents a potential therapeutic target for RA.

Sema4D in rheumatoid arthritis.

Introduction

Rheumatoid arthritis (RA) is a common autoimmune disease that causes chronic inflammation of the synovium. RA synovitis evokes arthritic symptoms and leads to destruction of cartilage and bone in joints. Recent advances in pathogenesis of RA have revealed that complex interplays among genetic and environmental factors evoke autoimmunity, accompanied by the production of critical autoantigens such as citrullinated proteins (1, 2). Once RA is developed, autoimmunity is sustained and leads to persistent synovitis, which in turn causes destruction of bone and cartilage (3, 4). The mechanisms of sustained synovitis remain unclear. Recently, pro-inflammatory cytokines such as tumor necrosis factor α (TNF-α) and interleukin-6 (IL-6) were shown to play key roles in RA. Biological disease-modifying anti-inflammatory drugs (bDMARDs), which can block these cytokines, constitute the current standard of care (5, 6). However, a substantial proportion of RA patients couldn't still achieve drug-free remission of bDMARDs. In order to achieve true remission, it will be necessary to identify another key molecular player that contributes to autoimmunity, immune activation, and bone destruction in RA.

Semaphorins were originally identified as neural guidance factors (7). The semaphorin family consists of more than 20 proteins, categorized into eight subclasses based on their structural features (8). Recent research on semaphorins demonstrated that these proteins play pleiotropic roles, including regulation of immune responses (9, 10), angiogenesis (11, 12), tumor metastasis (13, 14), and bone metabolism (15-17). The semaphorins involved in various aspects of immune responses are referred to as "immune semaphorins" (18). Previous reports have shown that immune semaphorins play important roles in immunological disorders, including multiple sclerosis (MS),

Sema4D in rheumatoid arthritis.

airway hypersensitivity, granulomatosis with polyangiitis (GPA), and RA (9, 10). For instance, soluble Sema4A is elevated in sera of MS patients, in which Th17 cell populations are also increased (19). Recently, a *Sema6A* gene variant was identified as significant contributor to the risk of GPA (20). In addition, serum levels of Sema3A and Sema5A have been suggested to be relevant to RA (21-23). However, the pathological significance of semaphorins in autoimmunity remains unclear.

Semaphorin 4D/CD100 was the first semaphorin shown to play a role in the immune system (24-26), and was identified originally as a T-cell activation marker (24). Indeed, Sema4D is abundantly expressed on the cell surface of T cells (24); however, it is also expressed in a broad range of hematopoietic cells. Although Sema4D is a membrane-bound protein, it also exists as a functional soluble form (sSema4D) following proteolytic cleavage upon cellular activation (27, 28). Sema4D binds several receptors, plexin-B1/B2, CD72, and plexin C1, which mediate the effects of Sema4D on neural cells, immune cells, endothelial cells, and epithelial cells (25, 29). Several studies have demonstrated that Sema4D plays crucial roles in the immune system, e.g.: i) Sema4D promotes activation and antibody production by B cells (30); ii) Sema4D expressed on dendritic cells (DCs) is involved in antigen-specific T-cell priming (31); iii) Sema4D induces cytokine production by monocytes (32); and iv) Sema4D mediates retrograde signals in mediating restoration of epithelium integrity (29).

Several studies have shown that Sema4D is relevant to the pathogenesis of autoimmunity. For instance, Sema4D-deficient mice are resistant to the development of experimental autoimmune encephalomyelitis (EAE) (33), a murine model of MS. Sema4D is expressed on tumor-associated macrophages (TAMs), and Sema4D produced by TAMs is involved in tumor angiogenesis and vessel maturation (34).

Sema4D in rheumatoid arthritis.

Notably, Sema4D derived from osteoclasts suppresses bone formation by osteoblasts, and blocking of Sema4D results in increased bone mass (15). Immune abnormality, angiogenesis, and bone destruction all play critical roles in the progression of RA (35, 36), suggesting that Sema4D might exacerbate RA. However, the involvement of Sema4D in the pathogenesis of RA has not yet been determined.

In this study, we found that sSema4D levels were elevated in sera and synovial fluids from RA patients. The increased levels of sSema4D were produced by an inflammation-related proteolytic mechanism, and the resultant sSema4D in turn induced inflammation, suggesting the existence of an inflammatory activation loop in RA synovium. Inhibition of Sema4D ameliorated the symptoms of collagen induced arthritis (CIA). These results suggest that Sema4D represents a potential target for treatment of RA.

Materials and methods

Patients

Biological samples from 101 patients with RA, 34 with systemic lupus erythematous (SLE), 10 with ankylosing spondylitis (AS), and 10 with osteoarthritis (OA) were obtained at Osaka University Hospital and National Hospital Organization Osaka Minami Medical Center. Patients with RA were diagnosed according to the American College of Rheumatology (ACR) 1987 criteria (37). Blood samples from healthy individuals were recruited from university staff, hospital staff, and students. Seven RA and ten OA synovial tissue samples were obtained from patients undergoing synovectomy or knee replacement, and RA and OA synovial fluids were collected from patients undergoing knee arthrocentesis. All samples were collected after informed

Sema4D in rheumatoid arthritis.

consent was obtained from the subjects, in accordance with the Declaration of Helsinki, and with approval from the Local Ethics Committee of Osaka University Hospital and National Hospital Organization Osaka Minami Medical Center. This study was registered in UMIN-CTR (UMIN000013076).

Enzyme-linked immunosorbent assays (ELISA).

Soluble Sema4D levels in sera, synovial fluids, and cell culture supernatants were measured using an ELISA kit (MyBioSource, San Diego, CA, USA). Serum and synovial fluid samples were stored at −20 °C prior to ELISA evaluation. The lower detection limit of sSema4D was 125 pg/mL. Levels of ADAMTS4 (a disintegrin and metalloproteinase with thrombospondin motif 4) in sera and synovial fluids were also determined using an ELISA kit (MyBioSource). The concentrations of human TNF-α and IL-6 in culture supernatants were determined using the Duoset ELISA kits for each cytokine (R&D Systems).

Histology

Immunohistochemical staining was performed on 7 RA and 10 OA synovial tissue samples. Briefly, sections were deparaffinized and subjected to antigen retrieval by autoclaving in 10 mM citrate buffer (pH 6.0) for 15 minutes at 125 °C, after which endogenous peroxidase activity was blocked with Dako REAL™ peroxidase blocking solution (Dako, Glostrup, Denmark). The sections were allowed to react overnight with a mouse anti-Sema4D polyclonal antibody (1:100; BD Biosciences, San Jose, CA, USA), mouse anti-CD3 monoclonal antibody (1:100; Dako), mouse anti-CD20 monoclonal antibody (1:1; ready to use, Dako), and mouse negative-control Ig cocktail

Sema4D in rheumatoid arthritis.

(1:1; ready to use, Dako) or rabbit CD31 polyclonal antibody (1:50, Abcam, Cambridge, UK). The slides were then incubated with a peroxidase-labeled polymer conjugated to secondary anti-rabbit antibodies using EnVisionTM1/HRP (Dako), and then developed with 3,3'-deaminobenzidine as the chromogen.

Histological analyses of joints were performed in mouse CIA. Hindlimb specimens from mice were fixed in 4% paraformaldehyde (Wako Pure Chemical, Osaka, Japan) and decalcified. Hematoxylin and eosin (H&E) and Safranin O stain were used to assess the synovitis.

Cell preparations

Human peripheral blood mononuclear cells (PBMCs) were separated by density-gradient centrifugation using Ficoll-Paque PLUS (GE Healthcare Bio-Sciences). $CD14^+$ monocytes were collected using CD14 MicroBeads (Miltenyi Biotec), yielding > 90% $CD14^+$ cells.

Flow cytometry

PBMCs were prepared in heparinized tubes by Ficoll-Paque density gradient centrifugation, and then analyzed on a FACS Canto (BD Biosciences) using the FlowJo software (Tree Star, Ashland, OR, USA). To prevent nonspecific binding, cells (2×10^5) were incubated with Human AB serum (Lonza, Basel, Switzerland) for 45 minutes at 4 °C, and then labeled with antibodies against indicated cell-surface antigens. The following antibodies were used: FITC-conjugated anti-human Sema4D antibody (A8; BioLegend), PE-conjugated anti-human CD3 (HIT3a; BioLegend), PE-conjugated anti-human CD14 antibody (M5E2; BioLegend), and PE-conjugated anti-human CD19

Sema4D in rheumatoid arthritis.

antibody (HIB19; Tonbo Biosciences, San Diego, CA, USA).

Quantitative reverse-transcription polymerase chain reaction (qRT-PCR)

CD3-, CD19- or CD14-positive cells (1×10^4) were sorted by FACSAria (BD Biosciences). Total RNA was extracted using the RNeasy Mini Kit (Qiagen), and cDNA was synthesized using the Super Script II cDNA synthesis kit (Invitrogen). qRT-PCR analysis was performed on a 7900HT Fast Real-Time PCR system (Applied Biosystems, Foster City, CA, USA) using the TaqMan PCR protocol. Assay IDs for TaqMan primer sets (Applied Biosystems) were Hs00174819_m1 for human *Sema4D* and HS00192708_m1 for human *ADAMTS4*. The expression levels of the tested genes were normalized to that of the housekeeping gene *ACTB* (Hs01060665_g1) and calculated using the ΔCt method.

Shedding of sSema4D

Monocytic cell line THP-1 and PBMCs from RA patients were cultured at 37 °C for 12 hours in 96-well plates at a density of 5×10^6 cells/ml in RPMI medium containing 10 μg/ml of matrix metalloproteinase 3 (MMP3) (Sigma-Aldrich, Milwaukee), matrix metalloproteinase 9 (MMP9) (R&D Systems), ADAM17 (a disintegrin and metalloproteinase 17) (R&D Systems), and ADAMTS4 (R&D Systems). sSema4D concentrations were measured using an ELISA kit (MyBioSource, San Diego, CA, USA).

Isolation of synovial cells and stimulation by IL-6 and TNF-α

Samples of knee articular synovium were obtained from RA patients. Synovial

Sema4D in rheumatoid arthritis.

tissues were chopped finely, and then digested for 45 minutes with continuous stirring at 37 °C with collagenase D (800 Mandl units/ml; Roche, Basel, Switzerland) and dispase I (10 mg/ml; Invitrogen) in RPMI 1640 medium containing 5% FCS. After digestion, the samples were filtered through a cell strainer (BD Biosciences). Adherent synovial cells were harvested and passaged into another dish. For experiments, synovial cells at passage 2–3 were seeded in 96 well-plates at 1×10^5 cells per well, and then stimulated for 2 days with 1 μg/ml of IL-6 and 0.1 μg/ml of TNF-α (Peprotech, London, UK) in DMEM containing 10% FCS. At the end of the stimulation period, cells were collected, and mRNA was extracted. qRT-PCR analysis of ADAMTS4 was performed on as described above. The concentrations of ADAMTS4 in culture supernatants were also measured by ELISA.

Monocyte culture and cytokine assays

$CD14^+$ monocytes from RA patients (1×10^5) were stimulated with or without various concentrations of soluble human Sema4D-Fc, naturally cleaved sSema4D, or anti-CD72 agonistic antibody (BU40, Santa Cruz Biotechnology). For blocking experiments, cells were co-cultured with 1 μg/ml of naturally cleaved Sema4D and 10 μg/ml of anti-Sema4D (CD100) antibody (3E9) or isotype-matched control IgG for 48 hours. The concentrations of human TNF-α and IL-6 in culture supernatants were determined by ELISA.

Human Sema4D-Fc and sSema4D were produced and purified as previously described (28, 32), and human IgG_1 Fc protein (R&D Systems) was used as a control. Naturally cleaved sSema4D was affinity purified using a column containing CNBr-activated Sepharose 4 Fast Flow resin (Amersham Pharmacia Biotech)